

Variational Shape Inference for Grasp Diffusion on $SE(3)$

S. Talha Bukhari, Kaivalya Agrawal, Zachary Kingston, and Aniket Bera

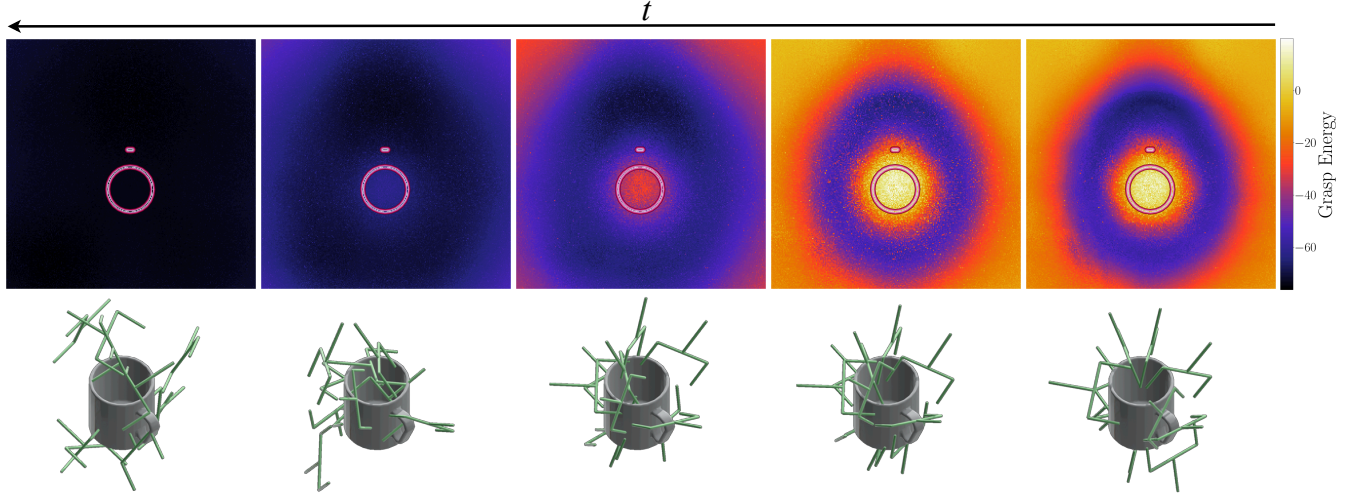


Fig. 1: Our energy-based formulation for Score Matching with Langevin Dynamics learns a time-conditioned grasp energy field. The time evolution of the learned energy field (*top row*) progresses through inverse Langevin dynamics (*left to right*) alongside the corresponding evolution of grasp samples (*bottom row*). Solid lines indicate the near-zero level sets of the object. The energy field visualization represents the solution to the grasp orientation optimization problem evaluated at every point on a 256×256 grid.

Abstract—Grasp synthesis is a fundamental task in robotic manipulation which usually has multiple feasible solutions. Multimodal grasp synthesis seeks to generate diverse sets of stable grasps conditioned on object geometry, making the robust learning of geometric features crucial for success. To address this challenge, we propose a framework for learning multimodal grasp distributions that leverages variational shape inference to enhance robustness against shape noise and measurement sparsity. Our approach first trains a variational autoencoder for shape inference using implicit neural representations, and then uses these learned geometric features to guide a diffusion model for grasp synthesis on the $SE(3)$ manifold. Additionally, we introduce a test-time grasp optimization technique that can be integrated as a plugin to further enhance grasping performance. Experimental results demonstrate that our *shape inference for grasp synthesis* formulation outperforms state-of-the-art multimodal grasp synthesis methods on the ACRONYM dataset by 6.3%, while demonstrating robustness to deterioration in point cloud density compared to other approaches. Furthermore, our trained model achieves zero-shot transfer to real-world manipulation of household objects, generating 34% more successful grasps than baselines despite measurement noise and point cloud calibration errors.

I. INTRODUCTION

The pursuit of autonomous robots entails sensing, planning, and interaction in the 3D world. Due to the increase in demand for robotic operation in unstructured workspaces, meaningful object interaction has become one of the foremost goals of research in robotic manipulation [1]. Here, generating stable grasps is a key task in enabling robust

manipulation in the real world. Recent efforts for large-scale data collection have enabled data-driven approaches for robot manipulation [2, 3]. For learning to grasp, the primary mode of ingesting expert grasp data is via imitation learning [4–6].

Given an object’s geometry, there are typically multiple feasible grasp solutions; hence, it is of interest to encode the *multimodality* of the task and capture the entire solution set, which can be fine-tuned or sub-sampled based on task-specific criteria [7, 8]. Denoising diffusion models [9, 10] have gained significant popularity across computer vision [11–13], language modeling [14–16], robotics [17–19], and beyond, due to their ability to capture highly complex multimodal distributions without mode collapse. In this work, we leverage diffusion models to learn the distribution of stable grasps conditioned on object geometry.

Generating stable grasps requires understanding of object geometry to identify regions on the object where grasps are feasible. This geometric understanding should be robust and transferable to arbitrary shapes for generalization in novel scenarios. Thus, geometric understanding serves as a key precursor to grasp synthesis [6]. Recent advances in neural scene representations have enabled new approaches to parameterize geometry, such as implicit neural representations (INRs) [20]. Properties such as differentiability, smoothness, and resolution invariance with a small memory footprint make INRs attractive for robot motion planning tasks [21, 22]. The most common implicit scene representation in robotics applications is the signed distance field (SDF) [23, 24], which provides distance and gradients to the nearest obstacle surface. We encode geometric features in our grasp synthesis pipeline by learning neural SDFs conditioned

on object point clouds [25, 26].

To enable a robust, generalizable, and multimodal grasp synthesis framework, we propose an approach centered around robust geometry inference. Our pipeline uses learned geometric features for stable, multimodal grasp synthesis through a two-stage process. We first learn a variational shape encoding guided by INRs, which maps object point clouds to a shape-latent space that enables robust shape inference using imperfect observations. We then use the learned shape features for generating grasp poses via diffusion on the SE(3) manifold. Similar to Urain et al. [8], our framework can be directly incorporated into multi-objective optimization, allowing us to tune the generated grasp poses to include feasibility constraints. We demonstrate this capability by introducing a test-time optimization routine that uses a smooth, differentiable representation of the robot gripper to fine-tune the generated grasp poses for improved stability and success rates. We present results on noisy and sparse point clouds, and demonstrate the effectiveness of our method in real-world settings.

II. RELATED WORK

A. Multimodal Grasp Synthesis

In recent years, several methods have been proposed for generating a diverse set of grasps conditioned on object geometry. Mousavian et al. [7] propose a conditional variational autoencoder (cVAE) that learns to compress and reconstruct grasps conditioned on object point clouds. However, VAEs are known to exhibit mode collapse and failure in fully capturing the data distribution. To improve performance, this work couples the grasp generator with a grasp classifier, which is expensive to train.

Diffusion models have demonstrated improved multimodal distribution modeling and stable learning dynamics while avoiding mode collapse [27], leading to their emergence in robotics applications [17, 18]. Urain et al. [8]’s formulation is closest to ours, where a diffusion model is learned via denoising score matching guided by an object reconstruction cost, which represents the current state-of-the-art in multimodal grasp synthesis. Our framework better models geometric structure in the presence of noise and calibration errors by learning to project geometric observations to a latent space of shapes and using it to infer shape features to guide grasp synthesis.

Several recent works have extended diffusion-based grasp synthesis in various directions. Chen et al. [28] propose using stochastic interpolants to sample from an informed prior distribution instead of a Gaussian and *bridge* to the target distribution. Singh et al. [29] use a part-guided diffusion approach to generate grasps tailored to areas of interest instead of the whole object. Barad et al. [30] propose learning a latent space where diffusion on grasps is performed, and use language to condition on grasp regions. Carvalho et al. [31] propose a denoising diffusion probabilistic model for grasp synthesis, and optimize the grasps at test-time using collision spheres. Similarly, we propose a test-time grasp pose optimization technique that boosts performance without

additional training on expert grasps. Song et al. [32] present an approach combining dense prediction with multimodal grasp generation via diffusion models. Lim et al. [33] proposes a novel equivariant lifting layer for constructing SE(3)-equivariant time-dependent velocity fields in flow matching. However, it performs worse in our experience, possibly requiring a significantly longer training time to handle the set of challenging objects used in our setup.

B. Neural Shape Inference

Modern 3D shape representation methods have tackled shape inference from voxel grids [34], point clouds [35], and implicit representations [36]. Implicit neural representations (INRs), usually in the form of signed distance fields [20, 25, 37], have made their way into robotics tasks such as motion planning [22], scene understanding [21], and manipulation [38]. Synthesizing grasps entails understanding geometric features, and hence, learning robust shape representations is key precursor to inferring stable grasp distributions conditioned on shapes. It is desired that shape learning algorithms generalize to a wide variety of shapes and sizes [25, 39], and exhibit robustness to real-world noise and calibration errors. An approach to handle noisy observations is to learn a prior over a latent space of shapes [40]. Furthermore, using a probabilistic approach to infer shape features captures a broader set of plausible surfaces [41, 42] compared to point estimates from deterministic methods. We build on the work of Chou et al. [42] by learned a rich latent space of shapes conditioned on object point clouds, and using the inferred shape features to drive robust grasp synthesis.

III. BACKGROUND

A. Denoising Diffusion Models

Denoising diffusion models [10, 27, 43] are a class of generative models that, given sequentially corrupted data samples (forward process), learn to reverse this corruption to generate samples from the data distribution (reverse process). Here, we discuss the Denoising Score Matching with Langevin Dynamics (SMLD) approach to diffusion models [9], where we learn to estimate the score of the distribution at each noise scale, and then use Langevin dynamics to sample from progressively decreasing noise scales during generation.

Let $\rho_D(\mathbf{x})$ denote the data distribution, and we sample $\mathbf{x}_0 \sim \rho_D(\mathbf{x})$. The forward process reduces sampling from the noised distribution $q_k(\mathbf{x}_k) = \int_{\mathbf{x}} \mathcal{N}(\mathbf{x}_k | \mathbf{x}, \sigma_k^2 \mathbf{I}) \rho_D(\mathbf{x}) d\mathbf{x}$ to simply adding Gaussian noise to the data sample: $\mathbf{x}_k = \mathbf{x}_0 + \epsilon$ where $\epsilon \sim \mathcal{N}(\mathbf{0}, \sigma_k^2 \mathbf{I})$, $\sigma_k < \sigma_{k+1}$ for $k = 1, \dots, L$, and L denotes the number of noise scales. For the reverse process, the score function $\nabla_{\mathbf{x}_k} \log q_k(\mathbf{x}_k)$ is approximated by training an estimator s_θ via the score-matching objective [44]:

$$\frac{1}{2} \sum_{k=0}^L \mathbb{E} [\|s_\theta(\mathbf{x}_k, k) - \nabla_{\mathbf{x}_k} \log \mathcal{N}(\mathbf{x}_k | \mathbf{x}_0, \sigma_k^2 \mathbf{I})\|_1]. \quad (1)$$

The trained score model can be sampled via Annealed Langevin Dynamics [9]: $\mathbf{x}_{k-1} = \mathbf{x}_k + \frac{\alpha_k^2}{2} s_\theta(\mathbf{x}_k, k) + \alpha_k \epsilon$, where $\epsilon \sim \mathcal{N}(\mathbf{0}, \mathbf{I})$ and $\alpha_k > 0$ is a step-dependent

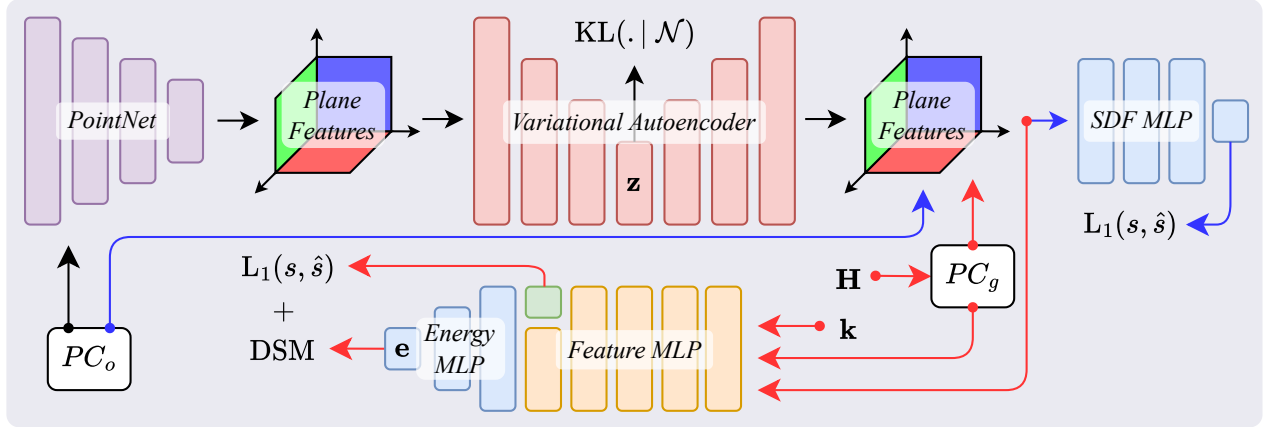


Fig. 2: Pipeline of our proposed approach for learning variational shape features for grasp diffusion. We first learn variational shape encodings by training a VAE-style architecture that reconstructs planar shape features for conditioning SDF MLP queries (*first row*). The learned shape encodings then condition the grasp diffuser by querying point cloud representations of gripper poses. DSM denotes the Denoising Score Matching objective and L_1 denotes the L_1 norm penalty. PC_o and PC_g denote object and gripper-attached point clouds, respectively. *Blue* and *red* arrows indicate training procedures for the *shape inference* and *grasp diffusion* stages, respectively.

coefficient. SMLD effectively learns a gradient vector field pointing toward high-density regions. An advantage of this formulation is that the score function does not depend on the generally intractable normalization constant of the underlying density function [45], making it easier to evaluate. In this work, we use SMLD to learn a generative model of grasp distributions conditioned on geometry.

B. Signed Distance Fields

Signed Distance Fields (SDFs) implicitly represent geometry by providing, at every point in space, the distance to the nearest surface, with a sign denoting the interior (negative) or exterior (positive). Formally, we let $\Omega(\mathbf{x}) : \mathbb{R}^3 \mapsto \mathbb{R}$ denote the signed distance field. The surface \mathcal{S} is then represented as the zero level-set of its SDF: $\mathcal{S} = \{\mathbf{x} \in \mathbb{R}^3 \mid \Omega(\mathbf{x}) = 0\}$. SDFs are differentiable almost everywhere, and where the gradient $\nabla_{\mathbf{x}}\Omega(\mathbf{x})$ exists, its negative points toward the nearest surface. Additionally, the gradient satisfies the Eikonal equation: $\|\nabla_{\mathbf{x}}\Omega(\mathbf{x})\| = 1$. In recent years, much work has focused on implicitly representing 3D geometries via neural SDFs [21, 25], where the SDF is parameterized by a neural network. This allows querying at arbitrary resolutions with a small memory footprint and readily yields gradients via automatic differentiation. In this work, we use signed distance fields to learn shape features, which we transfer to stable grasp synthesis. We also use a learned SDF of the robot gripper for test-time pose optimization of the gripper given object point cloud.

IV. METHODOLOGY

Our approach consists of three key components: (1) variational shape inference that learns geometric features from point clouds, (2) grasp synthesis via denoising score matching conditioned on these features, and (3) test-time pose optimization for enhanced grasp quality.

A. Shape Inference via Variational Autoencoding

High-quality grasp synthesis requires understanding geometric features that can transfer across object shapes and

be robust to imperfect observations. While inferring shape features from point clouds is an extensively researched task [39, 42, 46], multimodal frameworks that learn shape priors in a latent space offer superior robustness to observation noise and capture a broader space of plausible shape hypotheses [47, 48]. Following Chou et al. [42], we learn SDF representations from object point clouds using a PointNet-based variational autoencoder (PointVAE) architecture that encodes useful geometric priors.

To learn a continuous, complete, and sufficiently diverse latent space capable of modeling hundreds of shape categories and inferring their SDFs from unseen point clouds, we jointly train a conditional SDF network and a VAE. We use the architecture of Chou et al. [39], which can model SDFs of thousands of objects in a unified framework. The pipeline is comprised of a point cloud encoder Ψ that generates planar features $\pi = \Psi(X)$ from the input point cloud $X \in \mathbb{R}^{N \times 3}$. These features are processed by a VAE, Θ , to generate a latent vector z and reconstructed planar features $\hat{\pi}$: $[\hat{\pi}, z] = \Theta(\pi)$. The VAE compresses the latent space while a Gaussian prior regularizes it, enforcing continuity and completeness [49].

The reconstructed features $\hat{\pi}$ condition the SDF network Φ for predicting object-specific SDF values: $\hat{s} = \Phi(x \mid \hat{\pi})$, where $x \in \mathbb{R}^3$ is the query point. We learn geometric features by minimizing the L_1 loss on SDF values and the KL-divergence on the latent space distribution:

$$\mathcal{L}_S = \|\hat{s} - s\|_1 + \beta \cdot \text{KL}(q_\phi(z \mid \pi) \parallel p(z)),$$

where $s \in [-1, 1]$ denotes the ground truth SDF value at x , $q_\phi(z \mid \pi)$ represents the inferred posterior regularized to match the prior $p(z)$ (a zero-mean Gaussian), and $\beta = 10^{-5}$ controls the regularization strength.

B. Grasp Synthesis via Denoising Score Matching

Recent works on multimodal grasp synthesis [8, 31] use diffusion models to learn the distribution of stable grasps conditioned on object geometry. Following Urain et al. [8],

we use Denoising Score Matching (DSM) to learn the distribution of stable grasps conditioned on object geometry, leveraging our learned shape features.

Given a grasp pose $\mathbf{H} \in \text{SE}(3)$, we generate perturbed grasp poses by sampling perturbations from the Gaussian distribution on Lie groups:

$$q(\mathbf{H} \mid \mathbf{H}_\mu, \Sigma) \propto \exp\left(-\frac{1}{2} \|\text{Logmap}(\mathbf{H}_\mu^{-1}\mathbf{H})\|_{\Sigma^{-1}}^2\right),$$

where $\mathbf{H}_\mu \in \text{SE}(3)$ and $\Sigma \in \mathbb{R}^{6 \times 6}$ represent the mean and covariance, respectively. We obtain the perturbed grasp $\hat{\mathbf{H}} \sim q_k(\hat{\mathbf{H}}) = q(\hat{\mathbf{H}} \mid \mathbf{H}, \sigma_k \mathbf{I})$ via: $\hat{\mathbf{H}} = \mathbf{H} \cdot \text{Expmap}(\epsilon)$ where $\epsilon \sim \mathcal{N}(\mathbf{0}, \sigma_k^2 \mathbf{I})$ and $0 < k \leq L$ is the noise scale.

The model learns to estimate the score $\nabla_{\hat{\mathbf{H}}} \log q_k(\hat{\mathbf{H}})$ of the perturbed data distribution via the Score Matching objective [9, 45]:

$$\mathcal{L}_{\text{DSM}} = \frac{1}{L} \sum_{k=0}^L \mathbb{E}_{\mathbf{H}, \hat{\mathbf{H}}} \left[\left\| \mathbf{s}_\theta(\hat{\mathbf{H}}, k) - \nabla_{\hat{\mathbf{H}}} \log q_k(\hat{\mathbf{H}}) \right\|_1 \right],$$

where \mathbf{s}_θ denotes the score estimator parameterized by θ .

To enable composition with additional objective functions (e.g., our test-time pose optimization described in Sec. IV-C), we formulate an energy-based model E_θ by modeling the score function as $\mathbf{s}_\theta(\hat{\mathbf{H}}, k) = -\nabla_{\hat{\mathbf{H}}} E_\theta(\hat{\mathbf{H}}, k)$. Grasp synthesis proceeds by sampling $\mathbf{H}_L \sim q_L$ and running inverse Langevin dynamics in $\text{SE}(3)$:

$$\mathbf{H}_{k-1} = \text{Expmap}\left(\frac{\alpha_k^2}{2} \mathbf{s}_\theta(\mathbf{H}_k, k) + \alpha_k \epsilon\right) \mathbf{H}_k, \quad (2)$$

where $\epsilon \in \mathbb{R}^6$ is sampled from the multivariate standard normal and $\alpha_k > 0$ is a step-dependent coefficient. By running Eq. (2) for L steps, we obtain samples from the data distribution, corresponding to the grasp poses. Fig. 1 illustrates this process, showing the time evolution of the learned energy field during inverse Langevin dynamics along with the corresponding grasp sample evolution. We condition the grasp diffusion process on object geometry by querying the learned shape features $\hat{\pi}$ at gripper-attached point clouds, as illustrated in Fig. 2. We refer the reader to Solà et al. [50] for discussion and notation on Lie Groups.

C. Test-time Pose Optimization

The energy-based formulation enables incorporating additional cost functions during inference, which is particularly valuable when reliable environmental measurements are available. We introduce differentiable objective functions that capture intuitive grasping behaviors to drive generated grasps toward more stable poses.

We learn a neural SDF Ω_G of the robot gripper using the L_1 penalty on predictions and the Eikonal penalty on gradients (as described in Sec. III-B). Querying this neural SDF at object point clouds provides collision costs with differentiable gradients. We compose the queried SDF values $d(X \mid \mathbf{H})$ into a smooth differentiable collision avoidance objective: $\mathcal{L}_{\Omega_G}(\mathbf{H}) = \sum_X \exp(-\beta d(X \mid \mathbf{H})) - 1$. To encourage stable pinching configurations, we devise an objective that minimizes deviation from optimal gripper

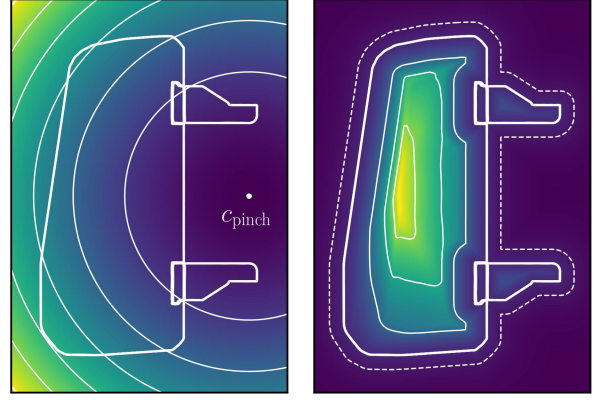


Fig. 3: Objective functions for test-time pose optimization: grasp pinch center alignment \mathcal{L}_c (left) and neural SDF of the gripper \mathcal{L}_{Ω_G} (right). These differentiable objectives guide generated grasps toward more stable configurations during inference.

positioning. We use object point clouds within and near the gripper's swept volume and penalize deviation of the centroid c_{bbox} of its axis-aligned bounding box from the grasp pinching center c_{pinch} : $\mathcal{L}_c(\mathbf{H}) = \sum_{c_{\text{bbox}}} (c_{\text{bbox}} - c_{\text{pinch}})^2$.

The combined objective $\mathcal{L}_{\text{opt}}(\mathbf{H}) = \gamma_1 \mathcal{L}_{\Omega_G}(\mathbf{H}) + \gamma_2 \mathcal{L}_c(\mathbf{H})$ is incorporated in the final (noise-free) stage of inverse Langevin dynamics:

$$\mathbf{H} = \text{Expmap}\left(\frac{\alpha_0^2}{2} (\mathbf{s}_\theta(\mathbf{H}, 0) + \nabla_{\mathbf{H}} \mathcal{L}_{\text{opt}}(\mathbf{H}))\right) \mathbf{H},$$

where $\beta, \gamma_1, \gamma_2 > 0$ balance the influence of the objective functions with the score function. In our experiments, we use $\beta = 10, \gamma_1 = 200, \gamma_2 = 200$. We employ the SIREN architecture [20] to model Ω_G due to its infinite differentiability and proven effectiveness for smooth, differentiable objectives [26].

D. Implementation Details

We employ a two-stage training procedure where shape feature learning precedes grasp synthesis. In the first stage, we train the shape autoencoder for surface reconstruction from object point clouds by coupling it with an SDF network regressor. We use the shape autoencoder from Chou et al. [42], which is composed of Convolutional PointNet encoders and decoders, while the SDF network employs the SIREN architecture [20].

Once pretrained, we couple the shape autoencoder to the energy-based model and train for grasp synthesis through denoising score matching. We use an MLP-style feature extractor similar to Park et al. [25] with the following modifications: 10 fully-connected layers interleaved with ReLU activation [51], weight normalization [52], and dropout [53]. Input features are propagated to even-numbered intermediate layers via FiLM-style conditioning [54] to balance learning capacity with memory costs. Noise-conditioning is implemented by mapping the noise level (scalar) to high-dimensional features using Gaussian Fourier Feature Projection [55]. The energy-based model comprises a two-layer ReLU-activated MLP that maps features from the feature extractor to scalar energy values. Our coupling mechanism

uses the standard data scale for the grasp diffuser while projecting data to the normalized point scale for the shape autoencoder, allowing the grasp synthesis pipeline to effectively be size-invariant. To promote $SO(3)$ -equivariance, we train our method with random rotations.

V. EXPERIMENTS

We evaluate our approach against state-of-the-art multimodal grasp synthesis frameworks: cVAE [7], SE(3)-Diff [8], Bridger [28], and GLDM [30]. All methods are trained on an NVIDIA A100 (40 GB) GPU for $\lesssim 48$ hours using ten object categories from the ACRONYM dataset [56]: Book, Bottle, Bowl, Cap, CellPhone, Cup, Hammer, Mug, Scissors, and Shampoo. We implement our method in PyTorch [57] and evaluate grasp success and stability in IsaacGym [58]. Additionally, we demonstrate zero-shot sim-to-real transfer on a pick-and-place task without additional training.

A. Shape Inference

Effective grasp synthesis requires robust geometric features that transfer across object shapes and remain stable under imperfect observations. To validate that our shape inference architecture (PointVAE) provides such features, we evaluate its surface reconstruction capabilities against a baseline approach. We train both our PointVAE-based encoder and a Vector Neurons [59] (VNN) encoder coupled with an MLP using an L_1 loss for object reconstruction on meshes from the ACRONYM dataset.

As shown in Tbl. I, the PointVAE backbone achieves superior reconstruction quality with lower Chamfer Distance (CD) and Unidirectional Hausdorff Distance (UHD) compared to the VNN encoder. The significantly lower failure rate in reconstructing the zero-level set with Marching Cubes surface extraction (4 vs. 42 failures) demonstrates that PointVAE better captures surface geometry. Crucially, learning a latent space of object geometries enables robust shape inference from limited observations, as we demonstrate in our point cloud sparsity experiments (Sec. V-C).

B. Grasp Synthesis

We evaluate grasp synthesis performance on 52 unseen object instances from the ACRONYM dataset, measuring average success rate (SR) and an empirical Earth Mover's Distance (EMD) with respect to the ground truth distribution as indicators of grasp quality and diversity, respectively. Tbl. II presents our main results, with corresponding distributions shown in Fig. 4.

Methods	Reconstruction Metrics \downarrow		Failures \downarrow (./7897)
	CD ($\times 10^{-2}$)	UHD ($\times 10^{-2}$)	
VNN [59]	11.07 \pm 06.85	23.43 \pm 18.25	42
PointVAE [42]	08.65 \pm 03.50	17.24 \pm 12.67	4

TABLE I: Shape inference performance comparing geometry reconstruction from point clouds. CD denotes *Chamfer Distance* and UHD denotes *Unidirectional Hausdorff Distance*. Failures indicates the number of failed surface extractions by the Marching Cubes algorithm [60].

Methods	Performance Metrics		
	S.R. (%) \uparrow	EMD \downarrow	Time (s) \downarrow
cVAE [7]	37.5 \pm 30.0	0.363 \pm 0.153	0.03 \pm 0.04
SE(3)-Diff [8]	79.0 \pm 17.9	0.176 \pm 0.058	1.63 \pm 0.13
Bridger [28]	80.2 \pm 23.9	0.189 \pm 0.055	0.14 \pm 0.04
GLDM [30]	64.7 \pm 25.3	0.300 \pm 0.096	7.39 \pm 0.20
Ours	86.5 \pm 20.9	0.192 \pm 0.067	2.05 \pm 0.13
Ours + GrOpt	88.5 \pm 14.6	0.193 \pm 0.072	3.12 \pm 0.51
w/VNN	78.3 \pm 19.8	0.189 \pm 0.046	1.73 \pm 0.17
w/VNN ⁺	82.5 \pm 20.1	0.190 \pm 0.052	1.79 \pm 0.11

TABLE II: Grasp synthesis performance on unseen object categories evaluated with IsaacGym simulation. S.R. denotes success rate computed over 10 sampled grasps per object. EMD (Earth Mover's Distance) is computed for 100 sampled grasps per object to measure diversity. Time indicates inference duration for sampling 200 grasps per object.

The cVAE baseline suffers due to training on a limited set of objects for grasp synthesis, while also demonstrating a lack of diversity due to mode collapse [8]. Furthermore, to boost its performance the cVAE depends on guidance from a grasp classifier [7] which is expensive to train. GLDM's emphasis on learning a latent grasp space, which we hypothesize is not needed due to already working in a low dimension, proves less effective. Although the SMLD formulation of SE(3)-Diff achieves reasonable performance, we believe it is limited by the VNN-based shape encoder. Bridger improves on SE(3)-Diff by employing stochastic interpolants, achieving a higher SR with significantly lower inference time. Our method achieves the highest success rate of 86.5%, outperforming the previous state-of-the-art by 6.3%, while maintaining competitive diversity (EMD = 0.192) and reasonable inference time ($\lesssim 2$ seconds).

Key to our performance is an improved grasp synthesis architecture, a robust latent space for shape feature learning, and pre-training the shape backbone for object reconstruction. To see that the improved grasp synthesis architecture alone does not contribute to this performance improvement, we train "w/VNN" which yields lower performance. We also show the usefulness of pre-training for learning shape features by training "w/VNN⁺", where the VNN is pre-

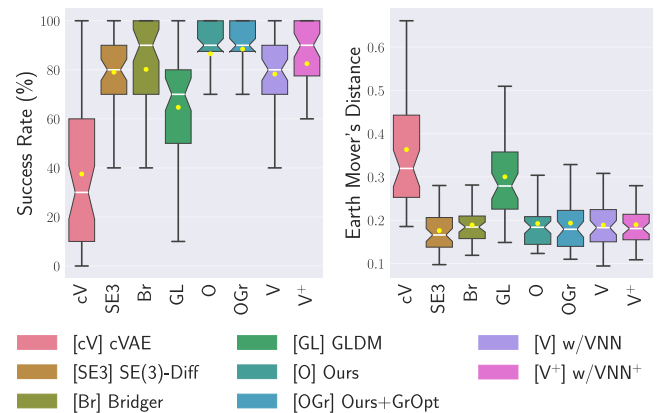


Fig. 4: Distribution of performance metrics corresponding to Tbl. II. Our method demonstrates the most consistent grasp performance across test objects while maintaining competitive grasp diversity.

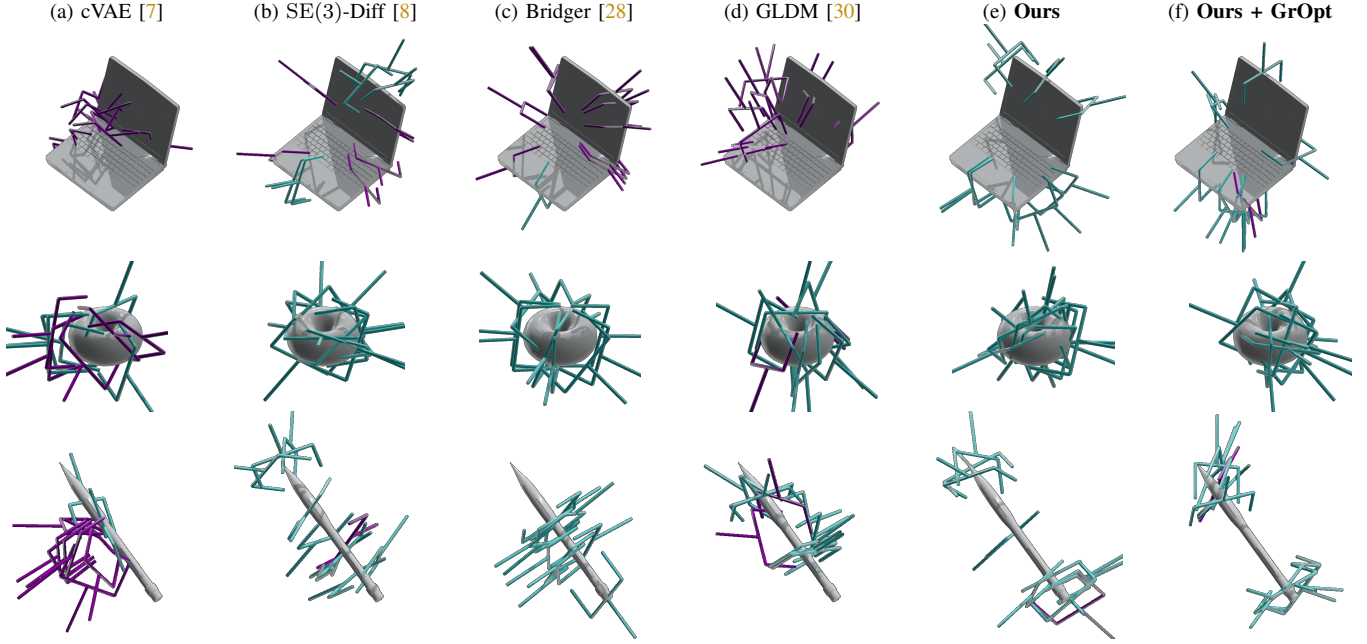


Fig. 5: Qualitative comparison of generated grasps for Laptop (*top row*), Donut (*middle row*), and Pencil (*bottom row*). **Dark cyan** indicates successful grasps while **dark purple** indicates failures. Compared to baselines, our method generates more successful and stable grasps across diverse object geometries as evaluated in IsaacGym.

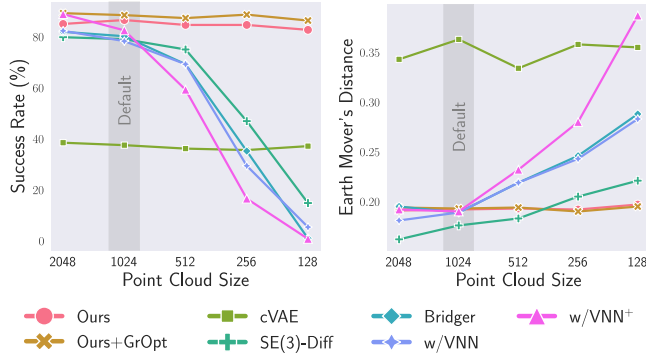


Fig. 6: Robustness evaluation under point cloud sparsity conditions. Baselines using standard PointNet-based encoders show deteriorating success rate (SR) and diversity (EMD) with increasing sparsity. Our variational shape inference approach maintains consistent performance across all sparsity levels.

trained via a surface reconstruction objective (described in [Sec. V-A](#)). Doing so boosts grasp synthesis performance compared to "w/VNN" but underperforms compared to Ours. This observation is supported by the shape inference results in [Sec. V-A](#). Finally, our proposed test-time pose optimization method (Ours + GrOpt) boosts success rate to 88.5% by encoding collision avoidance and pinch stability objectives. While this optimization slightly reduces diversity due to local refinement, it improves grasp quality and reduces variance. Qualitative results in [Fig. 5](#) illustrate the higher grasp quality achieved by our method across a diverse set of objects.

C. Point Cloud Sparsity

Real-world perception systems often produce sparse or noisy point clouds due to sensor limitations and environmental factors. We evaluate robustness by testing on point

clouds of varying density, from 128 to 2048 points, where the training default is 1024. We exclude GLDM in this analysis as it does not ingest point clouds of varying sizes. [Fig. 6](#) shows that methods using standard point cloud encoders experience significant performance degradation as point cloud sparsity increases. In contrast, our approach has consistent performance across all sparsity levels, with success rates remaining above 80% even with highly sparse inputs. This robustness stems from our variational shape inference, which learns a structured latent space that captures geometric priors and compensates for sparsity. This emphasizes the case for using the PointVAE architecture as a backbone for shape feature learning.

The cVAE baseline [7] also shows robustness due to its latent encoding, though at much lower performance. Notably, the pre-trained VNN encoder (w/VNN⁺) shows greater sensitivity to point cloud size than the non-pre-trained version, suggesting overfitting to the training point cloud density. Our test-time optimization maintains consistently high performance across all sparsity levels, demonstrating its effectiveness even with limited shape measurements.

Methods	Trials (·/10)				
	Book	Hammer	Jug	K-Bottle	Marker
cVAE [7]	0	0	0	0	0
SE(3)-Diff [8]	10	5	0	0	9
Bridger [28]	9	4	3	1	2
GLDM [30]	10	4	0	1	0
Ours	10	8	9	6	8

TABLE III: Zero-shot sim-to-real grasp synthesis results on household objects. Our approach demonstrates consistent performance across objects with varying geometries despite sensor noise and calibration errors in the real-world setting. K-Bottle denotes the Klein Bottle.

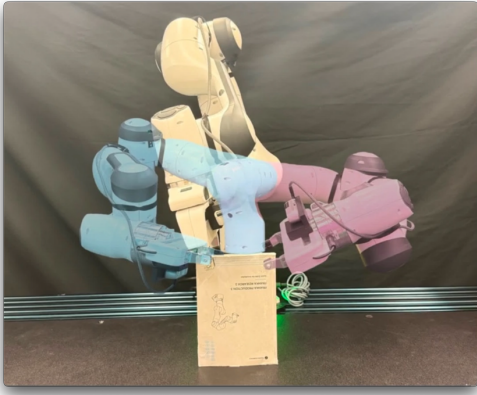


Fig. 7: Real-world grasp execution on a book using the Franka Research 3 robot arm. The demonstration showcases successful zero-shot transfer from simulation to real-world manipulation despite measurement noise and point cloud registration errors.

D. Real-world Deployment

To validate the effectiveness of our variational shape inference approach with real sensor data, we deploy our method on a Franka Research 3 robot arm equipped with a Panda Hand gripper in a pick-and-place task. The experimental setup uses a Realsense D435i camera to capture the robot’s workspace, with segmented object point clouds extracted using SAM [61] as shown in Fig. 7. Collision-free trajectories to and from the generated grasp poses are computed using the RRT-Connect implementation from VAMP [62]. Video demonstrations are provided in the supplementary material.

All methods are deployed without additional training or fine-tuning, evaluating zero-shot sim-to-real transfer capabilities. As presented in Tbl. III, our method achieves consistently high performance across all test objects, with particularly robust results for challenging geometries such as the Jug and Klein Bottle (K-Bottle). The Jug is significantly larger compared to other objects, and the Klein Bottle features smoothly varying curvature and complex geometry. These challenging objects are further complicated by real-world factors such as sensor noise and point cloud registration errors. Such conditions create substantial difficulties for baseline methods that rely on standard point cloud encoders, while highlighting the advantages of our variational shape inference approach (trained only on noise-free point clouds), which maintains robust performance despite measurement error. This robustness directly validates our core hypothesis that learning structured geometric priors through variational autoencoding improves grasp synthesis.

VI. CONCLUSION

In this work, we bring together approaches from generative modeling and implicit neural representations to enable robust and generalizable grasp synthesis. We employ a shape inference formulation parameterizing SDFs conditioned on object point clouds, and use the learned model to formulate grasp synthesis via a denoising diffusion model. Our proposal achieves superior performance compared to the state of the art in multimodal grasp synthesis, and demonstrates

robustness in the presence of observation noise. Additionally, our test-time optimization technique further improves grasp quality without requiring additional training from expert data.

This work furthers the case for the usefulness of transferring approaches for geometry understanding to grasp synthesis [6]. The demonstrated robustness to point cloud sparsity and the successful real-world experiments underscore the practical value of variational shape inference for robotic manipulation. Therefore, in the future, large pretraining for shape inference may immediately be made useful for grasp synthesis in a few-shot manner [63].

REFERENCES

- [1] S. Garg, N. Sünderhauf, F. Dayoub, D. Morrison, A. Cosgun, G. Carneiro, Q. Wu, T.-J. Chin, I. Reid, S. Gould, P. Corke, and M. Milford, “Semantics for robotic mapping, perception and interaction: A survey,” *Foundations and Trends in Robotics*, vol. 8, no. 1–2, pp. 1–224, 2020.
- [2] J. Kim, H. Ren, and A. H. Qureshi, “Integrating active sensing and rearrangement planning for efficient object retrieval from unknown, confined, cluttered environments,” *arXiv preprint arXiv:2411.11733*, 2024.
- [3] Open X-Embodiment Collaboration, “Open X-Embodiment: Robotic learning datasets and RT-X models,” *arXiv preprint arXiv:2310.08864*, 2023.
- [4] K. Hsiao and T. Lozano-Perez, “Imitation learning of whole-body grasps,” in *IEEE/RSJ Int. Conf. on Intelligent Robots and Systems*, 2006, pp. 5657–5662.
- [5] S. Kumra, S. Joshi, and F. Sahin, “Antipodal robotic grasping using generative residual convolutional neural network,” in *IEEE/RSJ Int. Conf. on Intelligent Robots and Systems*, 2020, pp. 9626–9633.
- [6] Z. Jiang, Y. Zhu, M. Svetlik, K. Fang, and Y. Zhu, “Synergies between affordance and geometry: 6-dof grasp detection via implicit representations,” in *Robotics: science and systems*, 2021.
- [7] A. Mousavian, C. Eppner, and D. Fox, “6-DOF GraspNet: Variational grasp generation for object manipulation,” in *IEEE/CVF Int. Conf. on Computer Vision*, 2019, pp. 2901–2910.
- [8] J. Urain, N. Funk, J. Peters, and G. Chalkatzaki, “SE(3)-DiffusionFields: Learning smooth cost functions for joint grasp and motion optimization through diffusion,” in *IEEE Int. Conf. on Robotics and Automation*, 2023, pp. 5923–5930.
- [9] Y. Song and S. Ermon, “Generative modeling by estimating gradients of the data distribution,” in *Advances in Neural Information Processing Systems*, 2019.
- [10] J. Ho, A. Jain, and P. Abbeel, “Denoising diffusion probabilistic models,” in *Advances in Neural Information Processing Systems*, 2020, pp. 6840–6851.
- [11] P. Dhariwal and A. Nichol, “Diffusion models beat gans on image synthesis,” in *Advances in Neural Information Processing Systems*, 2021, pp. 8780–8794.
- [12] R. Rombach, A. Blattmann, D. Lorenz, P. Esser, and B. Ommer, “High-resolution image synthesis with latent diffusion models,” in *IEEE/CVF Conf. on Computer Vision and Pattern Recognition*, 2022, pp. 10 684–10 695.
- [13] R. Po, W. Yifan, V. Golyanik, K. Aberman, J. T. Barron, A. Bermario, E. Chan, T. Dekel, A. Holynski, A. Kanazawa, C. Liu, L. Liu, B. Mildenhall, M. Nießner, B. Ommer, C. Theobalt, P. Wonka, and G. Wetzstein, “State of the art on diffusion models for visual computing,” *Computer Graphics Forum*, vol. 43, no. 2, 2024.
- [14] X. Li, J. Thickstun, I. Gulrajani, P. S. Liang, and T. B. Hashimoto, “Diffusion-LM improves controllable text generation,” in *Advances in Neural Information Processing Systems*, 2022, pp. 4328–4343.
- [15] L. Zhang, A. Rao, and M. Agrawala, “Adding conditional control to text-to-image diffusion models,” in *IEEE/CVF Int. Conf. on Computer Vision*, 2023, pp. 3836–3847.
- [16] S. Gong, M. Li, J. Feng, Z. Wu, and L. Kong, “DiffUseq: Sequence to sequence text generation with diffusion models,” *arXiv preprint arXiv:2210.08933*, 2022.
- [17] M. Janner, Y. Du, J. Tenenbaum, and S. Levine, “Planning with diffusion for flexible behavior synthesis,” in *Int. Conf. on Machine Learning*, 2022, pp. 9902–9915.
- [18] J. Carvalho, A. T. Le, M. Baierl, D. Koert, and J. Peters, “Motion planning diffusion: Learning and planning of robot motions with

- diffusion models,” in *IEEE/RSJ Int. Conf. on Intelligent Robots and Systems*, 2023, pp. 1916–1923.
- [19] C. Chi, Z. Xu, S. Feng, E. Cousineau, Y. Du, B. Burchfiel, R. Tedrake, and S. Song, “Diffusion policy: Visuomotor policy learning via action diffusion,” *The Int. Journal of Robotics Research*, 2023.
 - [20] V. Sitzmann, J. Martel, A. Bergman, D. Lindell, and G. Wetzstein, “Implicit neural representations with periodic activation functions,” in *Advances in Neural Information Processing Systems*, 2020, pp. 7462–7473.
 - [21] J. Ortiz, A. Clegg, J. Dong, E. Sucar, D. Novotny, M. Zollhoefer, and M. Mukadam, “iSDF: Real-time neural signed distance fields for robot perception,” in *Robotics: Science and Systems*, 2022.
 - [22] S. T. Bukhari, D. Lawson, and A. H. Qureshi, “Differentiable composite neural signed distance fields for robot navigation in dynamic indoor environments,” in *Int. Conf. on Robotics and Automation*, 2025.
 - [23] H. Oleynikova, A. Millane, Z. Taylor, E. Galceran, J. Nieto, and R. Siegwart, “Signed distance fields: A natural representation for both mapping and planning,” in *RSS Workshop: Geometry and Beyond-Representations, Physics, and Scene Understanding for Robotics*, 2016.
 - [24] H. Oleynikova, Z. Taylor, M. Fehr, R. Siegwart, and J. Nieto, “Voxblox: Incremental 3D Euclidean signed distance fields for on-board MAV planning,” in *IEEE/RSJ Int. Conf. on Intelligent Robots and Systems*, 2017, pp. 1366–1373.
 - [25] J. J. Park, P. Florence, J. Straub, R. Newcombe, and S. Lovegrove, “DeepSDF: Learning continuous signed distance functions for shape representation,” in *IEEE/CVF Conf. on Computer Vision and Pattern Recognition*, 2019, pp. 165–174.
 - [26] G. Yang, S. Belongie, B. Hariharan, and V. Koltun, “Geometry processing with neural fields,” in *Advances in Neural Information Processing Systems*, 2021, pp. 22 483–22 497.
 - [27] Y. Song and D. P. Kingma, “How to train your energy-based models,” *arXiv preprint arXiv:2101.03288*, 2021.
 - [28] K. Chen, E. Lim, K. Lin, Y. Chen, and H. Soh, “Don’t start from scratch: Behavioral refinement via interpolant-based policy diffusion,” in *Robotics: Science and Systems*, 2024.
 - [29] G. Singh, S. Kalwar, M. F. Karim, B. Sen, N. Govindan, S. Sridhar, and K. M. Krishna, “Constrained 6-dof grasp generation on complex shapes for improved dual-arm manipulation,” in *IEEE/RSJ Int. Conf. on Intelligent Robots and Systems*, 2024, pp. 7344–7350.
 - [30] K. R. Barad, A. Orsula, A. Richard, J. Dentler, M. Olivares-Mendez, and C. Martinez, “GraspLDM: Generative 6-DoF grasp synthesis using latent diffusion models,” *IEEE Access*, 2024.
 - [31] J. Carvalho, A. T. Le, P. Jahr, Q. Sun, J. Urain, D. Koert, and J. Peters, “Grasp diffusion network: Learning grasp generators from partial point clouds with diffusion models in $SO(3) \times R^3$,” *arXiv preprint arXiv:2412.08398*, 2024.
 - [32] P. Song, P. Li, and R. Detry, “Implicit grasp diffusion: Bridging the gap between dense prediction and sampling-based grasping,” in *Annual Conf. on Robot Learning*, 2024.
 - [33] B. Lim, J. Kim, J. Kim, Y. Lee, and F. C. Park, “Equigraspflow: Se (3)-equivariant 6-dof grasp pose generative flows,” in *Conference on Robot Learning*, 2024.
 - [34] Z. Wu, S. Song, A. Khosla, F. Yu, L. Zhang, X. Tang, and J. Xiao, “3d shapenets: A deep representation for volumetric shapes,” in *CVPR*, 2015.
 - [35] C. R. Qi, H. Su, K. Mo, and L. J. Guibas, “Pointnet: Deep learning on point sets for 3d classification and segmentation,” in *CVPR*, 2017.
 - [36] Y. Xie, T. Takikawa, S. Saito, O. Litany, S. Yan, N. Khan, F. Tombari, J. Tompkin, V. Sitzmann, and S. Sridhar, “Neural fields in visual computing and beyond,” in *Computer Graphics Forum*, 2022, pp. 641–676.
 - [37] L. Mescheder, M. Oechsle, M. Niemeyer, S. Nowozin, and A. Geiger, “Occupancy networks: Learning 3D reconstruction in function space,” in *IEEE/CVF Conf. on Computer Vision and Pattern Recognition*, 2019, pp. 4460–4470.
 - [38] C. Quintero-Pena, W. Thomason, Z. Kingston, A. Kyriakidis, and L. E. Kavraki, “Stochastic implicit neural signed distance functions for safe motion planning under sensing uncertainty,” in *IEEE Int. Conf. on Robotics and Automation*, 2024, pp. 2360–2367.
 - [39] G. Chou, I. Chugunov, and F. Heide, “GenSDF: Two-stage learning of generalizable signed distance functions,” in *Advances in Neural Information Processing Systems*, 2022, pp. 24 905–24 919.
 - [40] P. Mittal, Y.-C. Cheng, M. Singh, and S. Tulsiani, “AutoSDF: Shape priors for 3D completion, reconstruction and generation,” in *IEEE/CVF Conf. on Computer Vision and Pattern Recognition*, 2022, pp. 306–315.
 - [41] L. Zhou, Y. Du, and J. Wu, “3D shape generation and completion through point-voxel diffusion,” in *IEEE/CVF Int. Conf. on Computer Vision*, 2021, pp. 5826–5835.
 - [42] G. Chou, Y. Bahat, and F. Heide, “Diffusion-SDF: Conditional generative modeling of signed distance functions,” in *IEEE/CVF Int. Conf. on Computer Vision*, 2023, pp. 2262–2272.
 - [43] J. Sohl-Dickstein, E. Weiss, N. Maheswaranathan, and S. Ganguli, “Deep unsupervised learning using nonequilibrium thermodynamics,” in *Int. Conf. on Machine Learning*, 2015, pp. 2256–2265.
 - [44] Y. Song, J. Sohl-Dickstein, D. P. Kingma, A. Kumar, S. Ermon, and B. Poole, “Score-based generative modeling through stochastic differential equations,” in *Int. Conf. on Learning Representations*, 2021.
 - [45] A. Hyvärinen, “Estimation of non-normalized statistical models by score matching,” *Journal of Machine Learning Research*, vol. 6, no. 4, 2005.
 - [46] P. Erler, P. Guerrero, S. Ohrhallinger, N. J. Mitra, and M. Wimmer, “Points2Surf learning implicit surfaces from point clouds,” in *European Conf. on Computer Vision*, 2020, pp. 108–124.
 - [47] Z. Zhao, W. Liu, X. Chen, X. Zeng, R. Wang, P. Cheng, B. Fu, T. Chen, G. Yu, and S. Gao, “Michelangelo: Conditional 3D shape generation based on shape-image-text aligned latent representation,” in *Advances in Neural Information Processing Systems*, 2023, pp. 73 969–73 982.
 - [48] J. Zhou, W. Zhang, B. Ma, K. Shi, Y.-S. Liu, and Z. Han, “UDIFF: Generating conditional unsigned distance fields with optimal wavelet diffusion,” in *IEEE/CVF Conf. on Computer Vision and Pattern Recognition*, 2024, pp. 21 496–21 506.
 - [49] N. Chen, A. Klushyn, F. Ferroni, J. Bayer, and P. Van Der Smagt, “Learning flat latent manifolds with vaes,” in *Int. Conf. on Machine Learning*, 2020, pp. 1587–1596.
 - [50] J. Solà, J. Deray, and D. Atchuthan, “A micro lie theory for state estimation in robotics,” *arXiv preprint arXiv:1812.01537*, 2018.
 - [51] V. Nair and G. E. Hinton, “Rectified linear units improve restricted boltzmann machines,” in *Int. Conf. on Machine Learning*, 2010, pp. 807–814.
 - [52] T. Salimans and D. P. Kingma, “Weight normalization: A simple reparameterization to accelerate training of deep neural networks,” in *Advances in Neural Information Processing Systems*, 2016.
 - [53] N. Srivastava, G. Hinton, A. Krizhevsky, I. Sutskever, and R. Salakhutdinov, “Dropout: a simple way to prevent neural networks from overfitting,” *Journal of Machine Learning Research*, vol. 15, no. 1, pp. 1929–1958, 2014.
 - [54] E. Perez, F. Strub, H. De Vries, V. Dumoulin, and A. Courville, “Film: Visual reasoning with a general conditioning layer,” in *AAAI Conf. on Artificial Intelligence*, 2018.
 - [55] M. Tancik, P. Srinivasan, B. Mildenhall, S. Fridovich-Keil, N. Raghuvaran, U. Singhal, R. Ramamoorthi, J. Barron, and R. Ng, “Fourier features let networks learn high frequency functions in low dimensional domains,” *Advances in Neural Information Processing Systems*, 2020.
 - [56] C. Eppner, A. Mousavian, and D. Fox, “Acronym: A large-scale grasp dataset based on simulation,” in *IEEE Int. Conf. on Robotics and Automation*, 2021, pp. 6222–6227.
 - [57] J. Ansel et al., “PyTorch 2: Faster machine learning through dynamic python bytecode transformation and graph compilation,” in *ACM Int. Conf. on Architectural Support for Programming Languages and Operating Systems*, 2024.
 - [58] V. Makovychuk, L. Wawrzyniak, Y. Guo, M. Lu, K. Storey, M. Macklin, D. Hoeller, N. Rudin, A. Allshire, A. Handa, and G. State, “Isaac Gym: High performance GPU-based physics simulation for robot learning,” *arXiv preprint arXiv:2108.10470*, 2021.
 - [59] C. Deng, O. Litany, Y. Duan, A. Poulenard, A. Tagliasacchi, and L. J. Guibas, “Vector neurons: A general framework for $SO(3)$ -equivariant networks,” in *IEEE/CVF Int. Conf. on Computer Vision*, 2021, pp. 12 200–12 209.
 - [60] W. E. Lorensen and H. E. Cline, “Marching cubes: A high resolution 3D surface construction algorithm,” in *Seminal Graphics: Pioneering Efforts That Shaped the Field*, 1998, pp. 347–353.
 - [61] A. Kirillov, E. Mintun, N. Ravi, H. Mao, C. Rolland, L. Gustafson, T. Xiao, S. Whitehead, A. C. Berg, W.-Y. Lo, P. Dollár, and R. Girshick, “Segment anything,” *arXiv preprint arXiv:2304.02643*, 2023.
 - [62] W. Thomason, Z. Kingston, and L. E. Kavraki, “Motions in microseconds via vectorized sampling-based planning,” in *IEEE Int. Conf. on Robotics and Automation*, 2024, pp. 8749–8756.
 - [63] V. Vosylius and E. Johns, “Instant policy: In-context imitation learning via graph diffusion,” in *Int. Conf. on Learning Representations*, 2025.